Correlative characterization to understand ferrite recrystallization in dual phase steels

Naik, Chavan Akash; Kumar, B. K.Sarath; Seekala, Harita; Janakiram, S.; Kestens, Leo A.I.; Gautam, Jai Prakash; Phani, P. Sudharshan

DOI
10.1016/j.matchar.2025.114951

Publication date
2025

Document Version
Final published version

Published in
Materials Characterization

Materials Characterization 223 (2025) 114951

Contents lists available at ScienceDirect

Materials Characterization

journal homepage: www.elsevier.com/locate/matchar

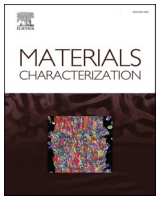

Correlative characterization to understand ferrite recrystallization in dual phase steels

Chavan Akash Naik [a], B.K. Sarath Kumar [b], Harita Seekala [b], S. Janakiram [a], Leo A.I. Kestens [c,d], Jai Prakash Gautam [a,*], P. Sudharshan Phani [a,*]

[a] School of Engineering Sciences and Technology, University of Hyderabad, India
[b] International Advanced Research Centre for Powder Metallurgy and New Materials (ARCI), Hyderabad, India
[c] Department of Electromechanics, Systems and Metals Engineering, Ghent University, Ghent, Belgium
[d] Materials Science and Engineering Department, Delft University of Technology, 2628 CD Delft, Netherlands

ARTICLE INFO

Keywords:
Advanced high strength steels
Dual phase steels
Ferrite recrystallization
Nanoindentation mapping
Electron microscopy
Clustering

ABSTRACT

A systematic experimental study has been carried out to understand ferrite recrystallization during isothermal annealing just below Ac1 in dual phase steels. Three different dual phase microstructures – ferrite-pearlite (FP), ferrite-bainite (FB) and ferrite-martensite (FM) were produced with an identical chemical composition. These samples were subjected to 80 % cold work and subsequently annealed at 725 °C for different soaking durations. The complex interaction between ferrite and secondary constituent/phase during deformation lead to differences in strain partitioning which influenced the kinetics of ferrite recrystallization. The sample with ferrite-martensite (FM) microstructure exhibited faster recrystallization kinetics followed by ferrite-bainite (FB) and ferrite-pearlite (FP). The microstructure and associated hardness evolution starting from cold rolling to annealing for different durations was carefully captured with electron back scattered diffraction (EBSD) and high-speed nano-indentation mapping. Excellent one-to-one correlation between hardness and KAM was observed by coupling EBSD-KAM and nanoindentation mapping. The effect of the secondary constituent/phase on ferrite recrystallization is presented and differences in the recrystallization kinetics are reconciled by correlative characterization. This work lays a foundation to link microstructure to the local mechanical response in dual phase steels and can be gainfully used to characterize multiphase steels and ultimately fine tune the processing.

1. Introduction

Steel has established itself as a critical and most acceptable material for automotive body parts. Specifically, dual-phase (DP) steels were the very first family of high strength automobile sheet steels with a great balance of ductility and strength ranging from 450 to 1200 MPa [1]. Hence, they are expected to be extensively used in the future as well, especially to achieve weight reduction and thereby enhanced fuel efficiency [1,2]. The ability to achieve ductility without compromising strength is determined by how well one can design the thermo-mechanical processing to achieve the desired size, shape, and distribution of the hard constituents in the soft matrix of the dual phase steels [3]. In this regard, ferrite-martensite is the first-choice dual phase candidate material that can provide excellent combination of strength and formability due to its load partitioning and hardening capability. Intercritical annealing (IA) is an established key step in obtaining the desired final dual phase microstructure. The ability to tailor the martensite size, volume fraction and distribution in the ferrite matrix after intercritical annealing and quenching is majorly driven by the initial microstructure, subsequent deformation and annealing (recrystallization and intercritical) conditions. Two processes are of prime importance in this regard- ferrite recrystallization and austenite formation [4]. As ferrite recrystallization and austenite formation can compete [5] with each other, especially at higher temperature, understanding each of these processes independently is critical. The focus of the current work is on ferrite recrystallization at a temperature close but below Ac1.

Prior work has reported that using martensite as the initial hard component of the dual phase microstructure (before intercritical annealing) followed by high heating rate to the IA temperature,

* Corresponding authors at: School of Engineering Sciences and Technology, University of Hyderabad, Prof. C.R. Rao road, Gachibowli, Hyderabad, Telangana 500046, India.
E-mail addresses: jaiprakashgautam@uohyd.ac.in (J.P. Gautam), spphani@uohyd.ac.in (P.S. Phani).

https://doi.org/10.1016/j.matchar.2025.114951
Received 30 December 2024; Accepted 19 March 2025
Available online 20 March 2025

enhances ferrite recrystallization and yields finer microstructure, which offers better properties [6,7]. In contrast, the microstructures which include other constituents such as ferrite-bainite-pearlite, and ferrite-pearlite with 50 % cold work resulted in slower recrystallization kinetics [8]. The energy stored within the material in the form of strain hardening due to prior deformation or due to the intrinsic processing is the driving force for recrystallization and phase transformation [9–11]. During deformation of the dual phase microstructure, typically the softer matrix has a greater tendency to accommodate strain and subsequently undergoes faster recrystallization. The accumulation of strain depends on various factors like the amount of deformation, size and distribution of the harder phase. Rana et al. [12] showed by digital image correlation (DIC) that deformation is localized in the soft matrix (ferrite) in dual phase steels. [13]. Also, the grain size and volume percentage of the hard phase such as martensite significantly influences load partitioning. Enhanced partitioning due to the hard phase occurs when its grain size is lower and volume fraction higher, which results in development of higher stress triaxiality, creating more opportunities to resist deformation [12,14]. Li et al. [15] showed that in case of ferrite, the fraction of recrystallized grains decreased and a delay in spheroidization of cementite in the pearlite lamellae was observed with increased heating rate. This is due to enhanced defect rearrangement, grain boundary mobility and carbon diffusion, all of which are temperature dependent transient phenomenon. Interestingly, during the early phase of recrystallization in dual phase deformed steels, an increase in hardness has also been reported due to formation of Cottrell atmosphere in a ferrite-pearlite microstructure [16,17].

In summary, the recrystallization phenomenon in dual-phase materials with different initial microstructures subjected to various processing conditions has been previously explored [4,5,9,10,18]. Additionally, prior work has focussed on determining the kinetic parameters through conventional methods which provides an overall response (matrix + secondary constituents) of the dual phase microstructure. However, a deeper understanding at the length scale of microstructure is essential, especially when the response of the different phases/constituents compete or overlap with one another during recrystallization process, wherein the conventional macroscale methods fail to deliver a concurrent understanding. Several processes such as accelerated / enhanced recovery, recovery suppression, bake hardening, partial / rapid / retarded recrystallization, spheroidization / precipitation, grain growth are all possible in dual phase steels. Hence, a systematic attempt is made in this study to understand some of these complex events with localized direct evidences from both structure (EBSD) and property evaluations (nanoindentation) in a widely used DP600 dual phase steel. A few recent works have demonstrated the ability to couple nanoindentation and EBSD to understand some key processing steps in dual phase steels such as hot rolling [18], early recovery [16,17], tempering [19]. etc. However, recrystallization has not been studied on similar lines. In addition, quantitative one-to-one correlation at the micrometer length scale has not been reported for these materials. Hence, in this work, three different dual phase microstructures: ferrite-pearlite (FP), ferrite-bainite (FB) and ferrite-martensite (FM) are produced with similar nominal composition. These are subjected to cold rolling followed by high temperature annealing close, but below Ac1 to understand the events during recrystallization by coupling electron microscopy and nanoindentation. The differences in the recrystallization kinetics of these three materials are presented and the underlying reasons are discussed. Overall, this work lays a foundation to link microstructure to the local mechanical response in dual phase steels and thereby provide insights on the recrystallization behaviour of dual phase steels by correlative characterization.

2. Materials and methods

2.1. Material processing

Steel with a nominal composition similar to DP 600 grade (0.09C, 1.65 Mn, 0.28 Si, <0.001 Nb and 0.057 Cr (all wt%)) was chosen as the starting material. Hot rolling was performed above austenite recrystallization temperature followed by cooling at different rates and coiling at different temperatures to obtain three distinct dual phase microstructures consisting of ferrite-pearlite (FP), ferrite–bainite (FB) and ferrite-martensite (FM). Further details of the processing conditions are available elsewhere [20]. These three materials were further subjected to 80 % cold rolling followed by annealing in salt bath at a temperature of 725 °C, which is below Ac1 (742 °C) with a heating rate of 185 °C/s, and soaking time of 10s, 60s 300 s and 900 s. The samples after different recrystallization annealing durations are labelled by appending the annealing time in seconds at the end of the initial microstructure label. For example, FB300 refers to the sample with ferrite-bainite (FB) microstructure that is annealed at 725 °C for 300 s.

2.2. Microstructural characterization

The samples were polished using SiC abrasive paper (grit sizes 400, 600, 800, 1000, 1200, 1500, 2000, and 2500), and then fine polishing was done by using vibrometer with a colloidal Silica suspension (size 0.04 μm) for at least 10 h. Subsequently samples were etched for phase identification using 2 % Nital solution that contains 2 % nitric acid and 98 ml of ethanol.

The microstructural investigations were performed using field emission scanning electron microscope (FESEM Model: FEI - NOVA NANOSEM450) with secondary electron imaging at an accelerating voltage of 20 kV and a working distance of 15 mm. Electron backscattered diffraction (EBSD) patterns were obtained at a step size of 0.1 μm using high-speed digital CCD camera (Digi View 5, TSL) and velocity pro detector. Kernel average misorientation was obtained using the 5th nearest neighbour and a maximum misorientation value of 3^{o}.

2.3. Mechanical characterization

Micro hardness of the specimen was measured using a micro Vickers hardness tester of Tinius Olsen (FH-006 series) make. The tests were carried out at a load of 500 g with a dwell time of 15 s. 25 indents were performed per specimen to determine the average hardness value. Local mechanical properties were obtained using high speed nanoindentation technique -NanoBlitz3D. This mapping was carried out using a commercially available nanoindenter, iMicro® with an InForce50 actuator from Nanomechanics Inc. (now KLA), Oak Ridge, USA. Indentation mapping was carried out on regions scanned by EBSD to enable one-to-one correlation between microstructure and local mechanical properties. A typical map has 3600 indents in a square grid pattern of 60 × 60 with a spacing of 1 μm. The maximum depth of indentation was limited to 100 nm to ensure a spacing to depth ratio of at least 10 as recommend in a previous work [21]. K-Means clustering was used to deconvolute the hardness data [22] to obtain the hardness values of the constituents.

3. Results

3.1. Microstructural evolution during isothermal annealing at 725 °C

Fig. 1 shows the SEM micrographs of cold rolled and subsequently annealed samples as a function of soaking time at 725 °C of the FP sample. The dual phase nature (ferrite-pearlite) is still distinct after cold deformation with elongated ferrite in the rolling direction and pearlite bands featuring fragmented cementite, as shown in Fig. 1 (a-b). Upon annealing, the cold rolled microstructure is retained up to a soaking time

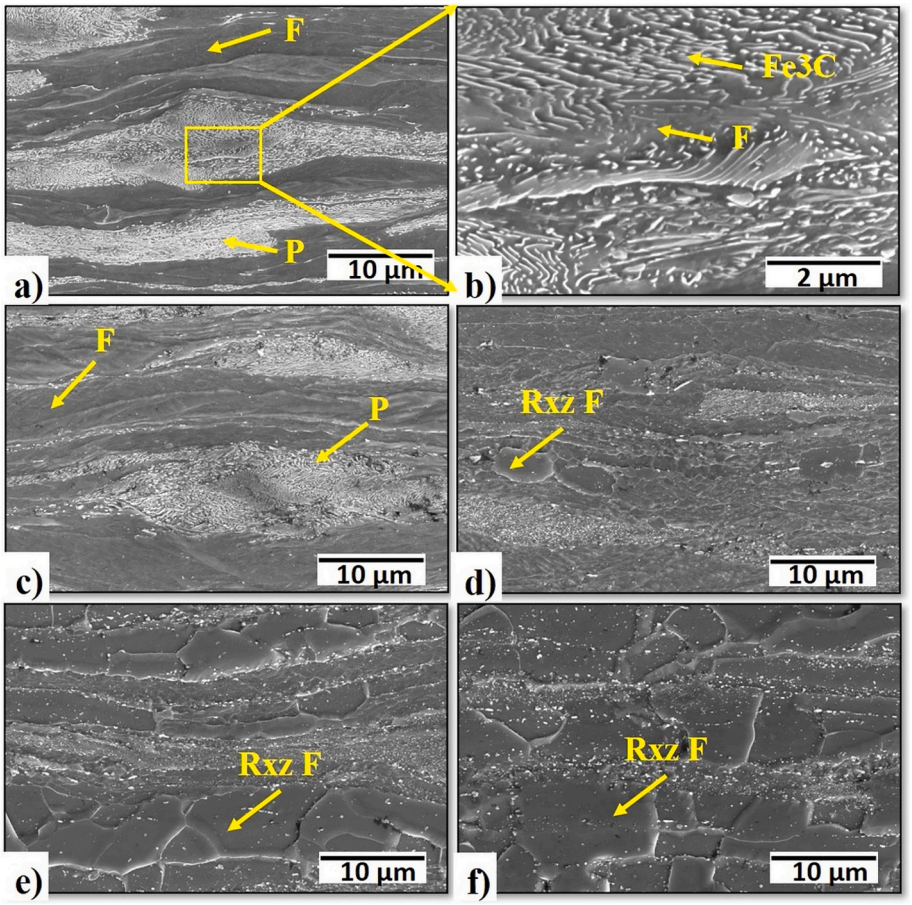

Fig. 1. SEM micrographs of ferrite-pearlite (FP) after (a, b) 80 % cold rolling and annealing at 725 °C for soaking periods of c) 10s d) 60s e) 300 s and f) 900 s.

of 10s, possibly corresponding to the early recovery. As the soaking duration increases to 60s, heterogeneity in ferrite grain sizes can be observed with sizes ranging from less than 1 μm to as large as 5–6 μm. With further soaking, the average ferrite grain size increases to 8.0 ± 1.2 μm after 300 s and 9.1 ± 0.7 μm after 900 s. Additionally, fine high-contrast features, most likely carbides, begin to appear and become increasingly prominent at longer soaking times. Furthermore, the banding patterns and deformation signatures completely disappear, while the density of carbides or clusters became more pronounced at higher soaking times.

In contrast, the microstructural evolution of ferrite-bainite (FB) and ferrite-martensite (FM) is distinctly different from ferrite-pearlite (FP) as shown in Fig. 2 (FB) and Fig. 3 (FM). Ferrite experiences substantial deformation, whereas bainite (Fig. 2a-b) and martensite show fragmentation (Fig. 3a-b). The FB microstructure shows residual deformation features after 10s of soaking at 725 °C, as seen in Fig. 2(c). However, the microstructure changes significantly after 60s of soaking, exhibiting distinct recrystallization characteristics, as shown in Fig. 2(d). The ferrite grains, which are fine and elongated after 10s of soaking, grow considerably to 6.2 ± 1.7 μm, 9.7 ± 1.2 μm and 11 ± 1.3 μm after 60s, 300 s and 900 s of soaking, respectively. Similar to the FP microstructure, fine high-contrast features, which could be carbides or clusters, are observed in the ferrite matrix after 60s of soaking. These features decrease in density and segregate to the grain boundaries and triple junctions of the ferrite grains with increasing soaking time, as shown in Fig. 2(e-f).

Similar to the case of FB, the FM microstructure shows distinct and uniform changes after 10s of soaking, as shown in Fig. 3(c). The ferrite phase maintains the deformation features until 10s, but not after 60s. The ferrite grain size also increases gradually, reaching 6.5 ± 1.3 μm, 9.8 ± 1.2 μm and 11 ± 1.9 μm after 60s, 300 s and 900 s of soaking, respectively. The carbides or clusters segregate to the grain boundaries, as evident from the micrographs of 300 s and 900 s in Fig. 3(e-f).

3.2. *Kernel average misorientation (KAM) evolution during isothermal annealing at 725 °C*

In addition to the microstructural evolution analysed from SEM micrographs (Figs. 1–3), EBSD-KAM based analysis is presented to quantify and compare the progress of recrystallization for the samples with different dual phase microstructures. KAM shows a single point's misorientation with respect to its neighbours and helps distinguish regions of low misorientation (strain-free grains) and high misorientation (deformed grains), thus enabling a better understanding of spatial distribution of recrystallization. Fig. 4 shows the spatial distribution of KAM (5th neighbour, $< 3°$ misorientation) for all materials at different soaking times. The misorientation levels observed in all materials are high in the cold rolled state, as expected and also after 10s of soaking time, suggesting that the deformation induced by cold rolling remains largely unaffected by the subsequent annealing for a short duration. With increasing soaking time, the FP sample exhibits a gradual decrease in misorientation in contrast to the FB and FM samples where a distinct drop in misorientation, especially in the ferrite matrix is observed at 60s, followed by the appearance of higher misorientations at specific regions such as triple points. This observation aligns with the microstructural observations, indicating the potential presence of carbides/clusters at triple points with elevated misorientations. These findings also suggest that the recrystallization kinetics are considerably faster in the case of FB and FM, reaching a saturation level in terms of recrystallization after 60s and subsequently forming carbides/clusters with prolonged

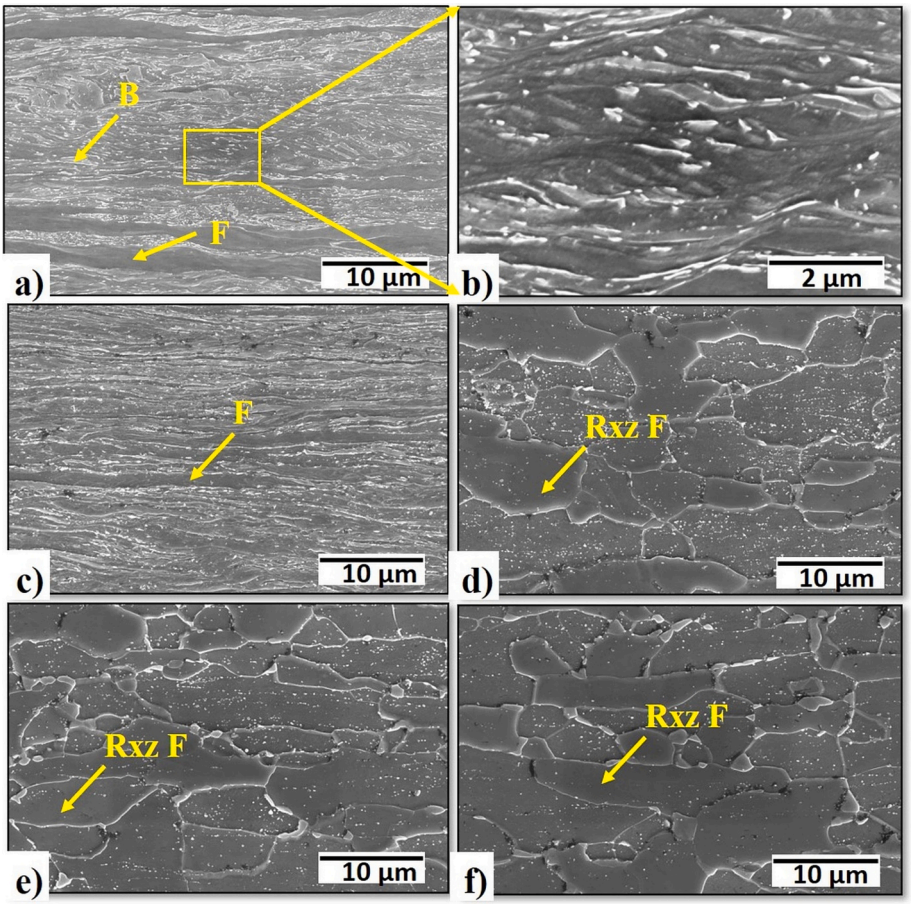

Fig. 2. SEM micrographs of ferrite-bainite (FB) after (a, b) 80 % cold rolling and annealing at 725 °C for soaking periods of c) 10s d) 60s e) 300 s f) 900 s.

annealing.

The EBSD-KAM maps shown in Fig. 4 can be further used to quantify the recrystallization kinetics. The recrystallization fraction (x) is determined by assuming that regions with KAM <1° are fully recrystallized and is plotted as a function of soaking time in Fig. 5(a). The fraction increases abruptly in the case of FB and FM unlike FP, where it increases gradually. This clearly shows that the recrystallization kinetics are much faster in the case of FB and FM compared to FP. To assess the underlying mechanism, the traditional Johnson and Mehl Avarami (JMAK) [23] equation shown below is assumed to model the kinetics of the recrystallization,

$$x = 1 - exp(-kt^n) \quad (1)$$

wherein, x is the recrystallization fraction, t is the annealing time, n is the exponent and k is the pre-exponential coefficient.

The double log plot of the recrystallization data shown in Fig. 5(a) in the case of FP is presented in Fig. 5(b). As the recrystallization is very fast in the case of FB and FM, such a plot is not feasible for those samples within the time scales chosen in this work. In the case of FP, clearly two distinct linear regions can be observed, indicating multiple concurrent processes. Disregarding the two distinct slopes, fitting a single slope by non-linear minimization with the standard JMAK equation for FP yields an exponent (n) of 1.1 and an activation energy (Q) of 288 KJ/mol, which is comparable to the self-diffusion activation energy in pure ferrite [24]. It may however be noted that the Q value thus determined may not be of much relevance due to the two distinct slopes but gives a qualitative indication of the underlying mechanism.

3.3. Microhardness evolution during isothermal annealing at 725 °C

Microhardness was determined at a load of 500 g for all the materials and is shown in Fig. 6, starting with the 80 % cold rolled state followed by annealing for different soaking durations. The initial hardness values after 80 % cold rolling are high compared to other states, as expected, with FM showing the highest hardness. As soaking duration increases, the hardness of FP exhibits a sharp decline to lower values after an initial rise. In contrast, in the case of FB and FM, the hardness shows a continuous decrease. Also, in the case of FP, the decrease in the hardness is gradual with respect to time unlike FB and FM, which show a drastic decrease after 10s and reach a constant lower value.

3.4. Nanoindentation hardness evolution during isothermal annealing at 725 °C

The micro hardness values presented in the previous section provide an overall response which covers both the ferrite matrix and the secondary constituents in a single indent due to the length scale of the indent. In order to determine the hardness of the individual constituents, nanoindentation mapping is performed on regions scanned by EBSD. In this section, the evolution of nanoindentation hardness at the micrometer length scale will be presented in the cold rolled state as well as after different soaking duration during isothermal annealing at 725 °C.

3.4.1. Ferrite-Pearlite (FP)

Fig. 7 shows the spatial distribution of hardness in FP after cold rolling and isothermal annealing for different soaking durations. The hardness maps show two major distinct regions - lower hardness (blue/cyan region) corresponding to ferrite and higher hardness corresponding

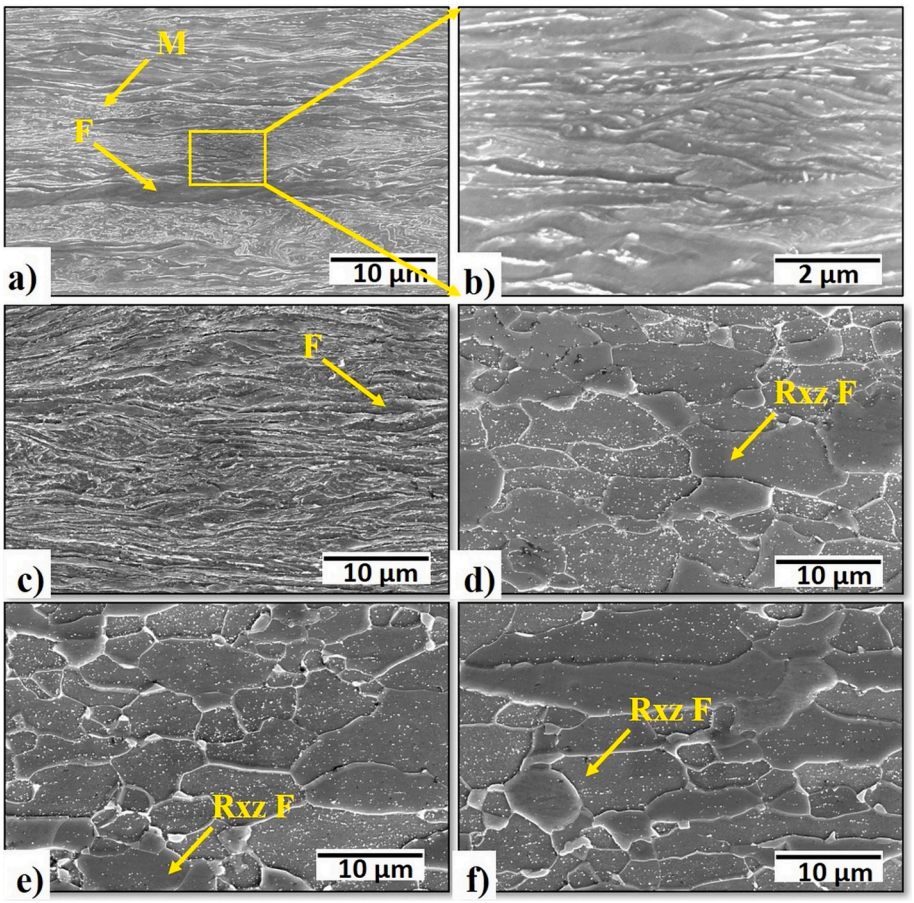

Fig. 3. SEM micrographs of ferrite-martensite (FM) after (a, b) 80 % cold rolling and annealing at 725 °C for soaking periods of c) 10s d) 60s e) 300 s f) 900 s.

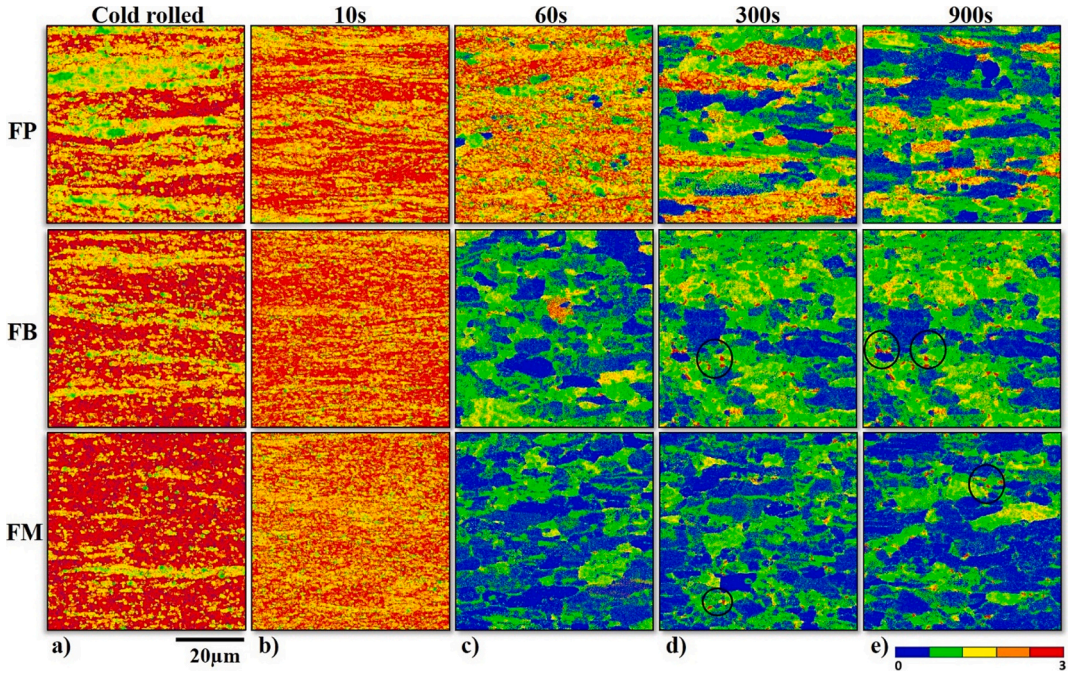

Fig. 4. KAM maps after (a) cold rolling and subsequent annealing at 725 °C for (b) 10s (c) 60s (d) 300 s and (e) 900 s.

to pearlite having a banded morphology. The mapping clearly captures the local variations in the hardness including the signatures of prior deformation. The cold rolled hardness levels are retained up to 60s of soaking time followed by a gradual decrease. The pearlite bands are not continuous at higher soaking times and the secondary constituents become less apparent. These observations are in qualitative agreement

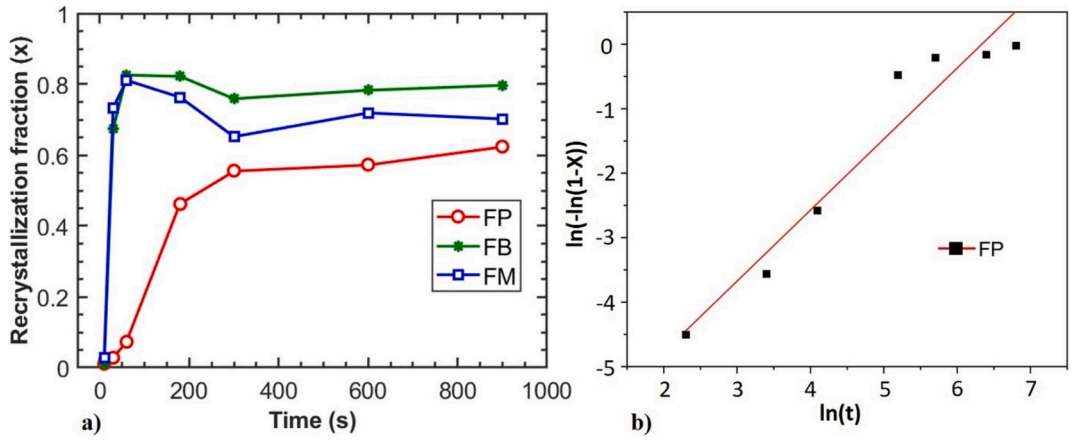

Fig. 5. (a) Recrystallization fraction as a function of soaking duration and (b) log-log plot of recrystallization kinetics of FP as per JMAK model.

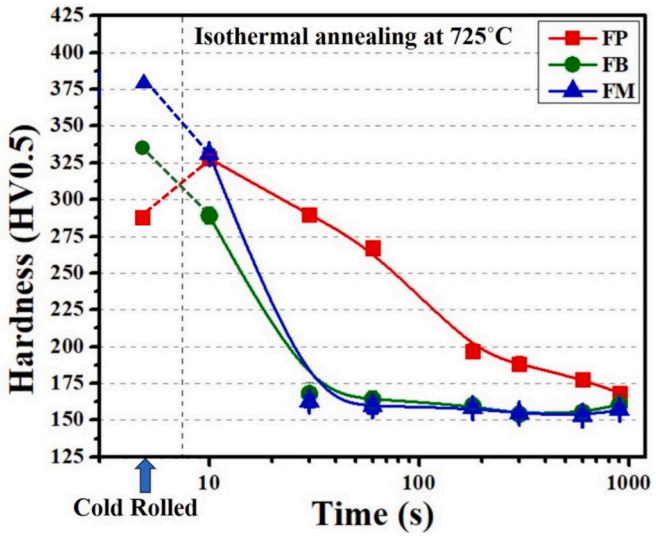

Fig. 6. Microhardness evolution in FP, FB and FM with soaking time at 725 °C.

with the microstructure presented in the previous section and a detailed comparison will be presented in the discussion section.

3.4.2. Ferrite-Bainite (FB)

Fig. 8 shows the spatial distribution of hardness in FB after cold rolling and isothermal annealing for different soaking durations. Similar to the case of FP, the hardness maps show two major distinct regions - lower hardness corresponding to ferrite and higher hardness corresponding to bainite. The cold rolled state exhibits higher hardness as expected, which is retained even after annealing for 10s. Upon further annealing for 60s, the map shows a drastic reduction in hardness. Annealing for longer durations (300 s and 900 s) results in small localized regions with high hardness in contrast to the case of FP. These regions correspond to the carbides/carbon rich clusters which are located specifically at boundaries, triple points and support the observations from SEM micrographs and misorientation maps presented earlier.

3.4.3. Ferrite-Martensite (FM)

Fig. 9 shows the spatial distribution of hardness in FM after cold rolling and isothermal annealing for different soaking durations. The response has many similarities with that of FB, In the cold rolled state, the hardness in the case of FM is higher than that of FB or FP. Subsequently, annealing even for 10s shows a decrease in hardness, while annealing to 60s results in significant drop in hardness. Also, as in the case of FB, clusters of high hardness regions appear after 300 s of soaking, which increase in number density after further annealing to 900 s.

4. Discussion

4.1. Structure property correspondence at the micrometer length scale

The data presented in the results section shows clear differences in the evolution of the microstructure and hardness during annealing of the different dual phase materials. The presence of multiple phases greatly complicates the understanding of the underlying reasons, which is the primary focus of this work. To help understand the underlying mechanisms during recrystallization of dual phase steels an attempt is made to correlatively track the evolution of microstructure and hardness at the micrometer length scale. Here we present the example of FP sample which has been cold rolled to 80 % followed by isothermal annealing at 725 °C for 300 s to demonstrate the quantitative correspondence between the microstructure and property. Fig. 10 shows the KAM map and the hardness map from a 60 × 60 μm^2 area in the sample, It may be noted that the inherent resolution of the EBSD-KAM map is much higher than that of the hardness map (~ 1 μm). Despite this, good correspondence between the KAM and hardness maps can be observed. Broadly, two distinct regions can be observed from the KAM map – low misorientation corresponding to recrystallized ferrite, and higher misorientation corresponding to unrecrystallized/partially recrystallized ferrite and pearlite or other secondary constituents. Similar trend can be observed in the case of hardness. To enable a quantitative comparison, the corresponding histograms obtained from the maps are also shown, which further confirm that the KAM and hardness show good one-to-one correspondence. Both the histograms show presence of two peaks; the lower one corresponding to the recrystallized ferrite matrix and the higher ones corresponding to unrecrystallized /partially recrystallized ferrite and pearlite. This observation leads to the need to compare the KAM and local hardness for all the samples all through the annealing process.

Fig. 11 shows a comparison of the KAM and hardness histograms of FP, FB and FM in the cold rolled (CR) state as well as after annealing for different durations as indicated by the number appended to the end of the sample name. For example, FB300 refers to the sample with ferrite-bainite (FB) microstructure that is cold rolled to 80 % and subsequently annealed at 725 °C for 300 s. The KAM and hardness maps show remarkable similarity in all the cases. The histograms show a general decrease in KAM and hardness from the cold rolled state with annealing, as expected. Also, the shift towards lower KAM or hardness is gradual in the case of FP compared to FB and FM indicating faster ferrite recrystallization in FB and FM. Interestingly, the histograms also show the

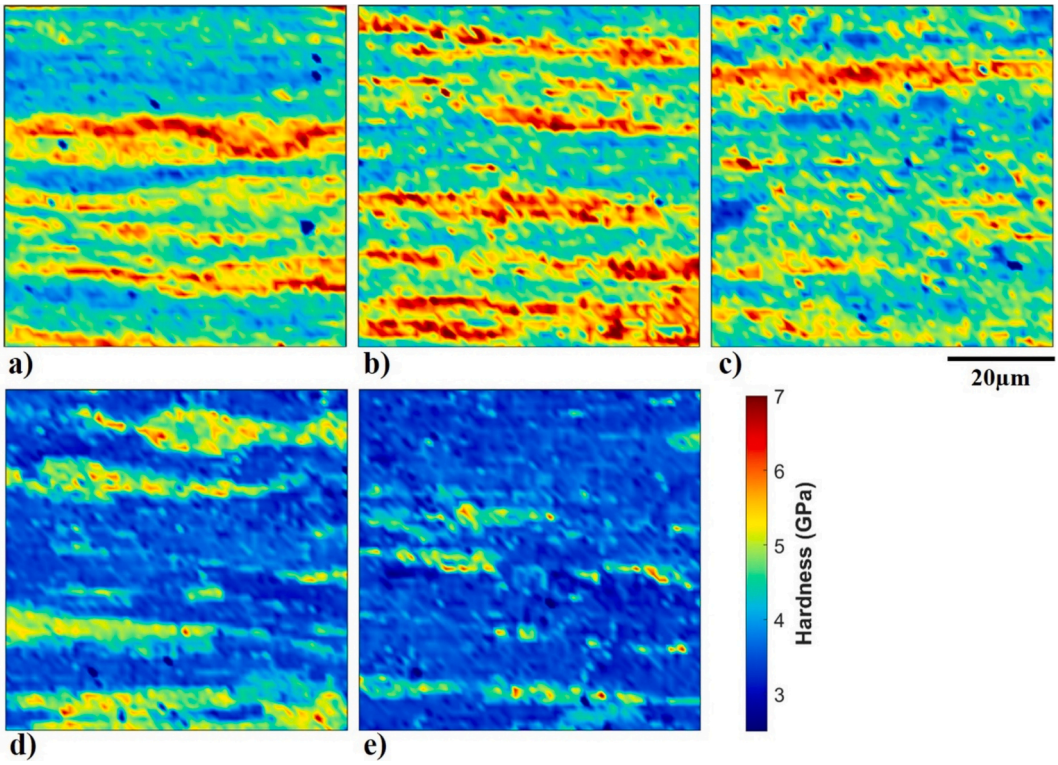

Fig. 7. Nanoindentation hardness maps of FP after (a) 80 % cold rolling followed by annealing at 725 °C for (b) 10s (c) 60s (d) 300 s and (e) 900 s.

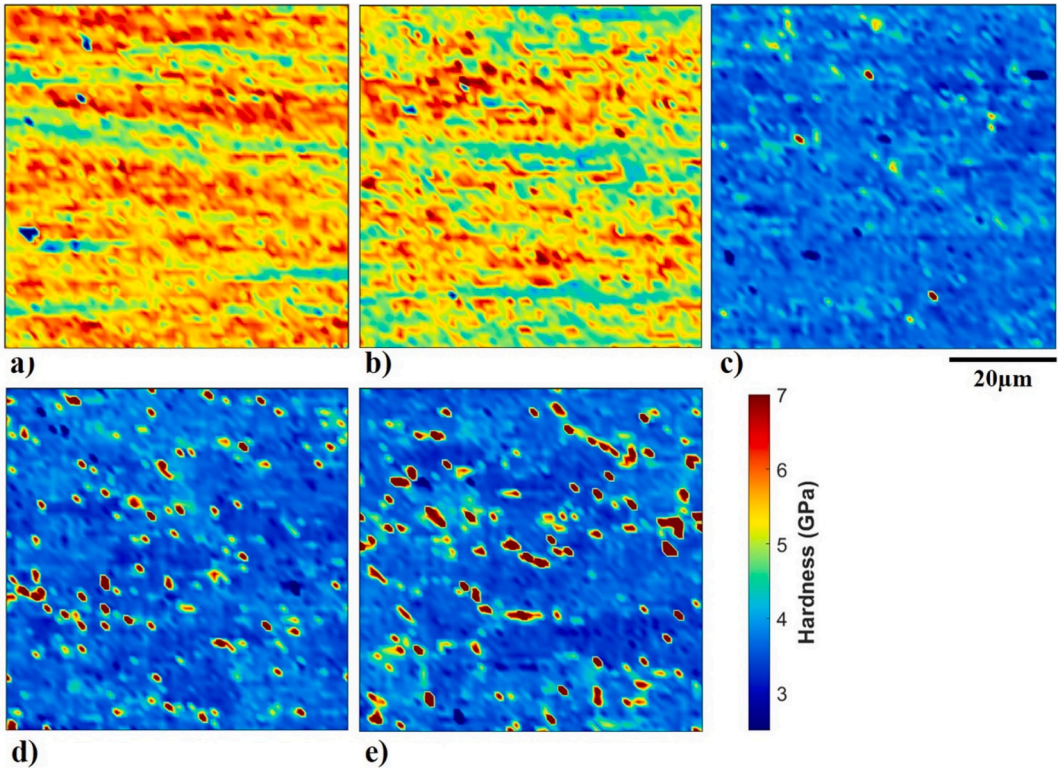

Fig. 8. Nanoindentation hardness maps of FB after (a) 80 % cold rolling followed by annealing at 725 °C for (b) 10s (c) 60s (d) 300 s and (e) 900 s.

emergence of a bimodal distribution with annealing in the case of FP and not in FB or FM. This can be attributed to the stability of the secondary constituent (pearlite) in the case of FP compared to bainite or martensite which are relatively less stable. The plot clearly establishes the ability of the nanoindentation mapping technique to capture the local variations in hardness at the length scale encountered in typical dual phase steels. The KAM histogram effectively reflects the internal microstructural changes, while the hardness histogram represents the corresponding

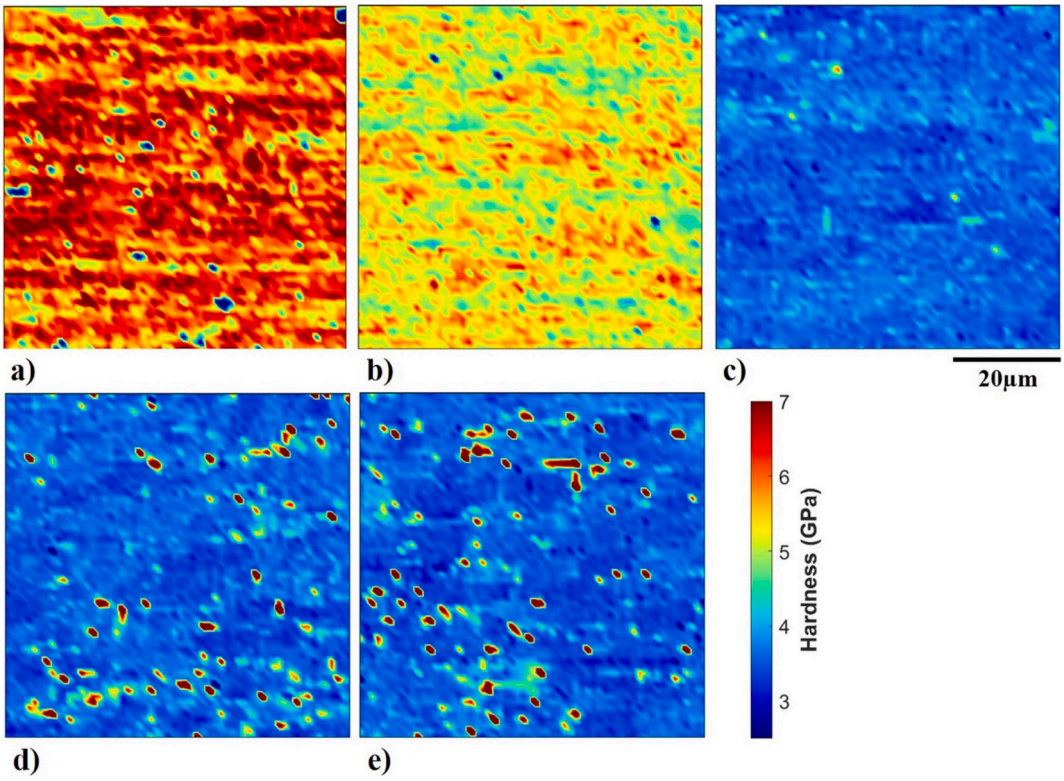

Fig. 9. Nanoindentation hardness maps of FM after (a) 80 % cold rolling followed by annealing at 725 °C for (b) 10s (c) 60s (d) 300 s and (e) 900 s.

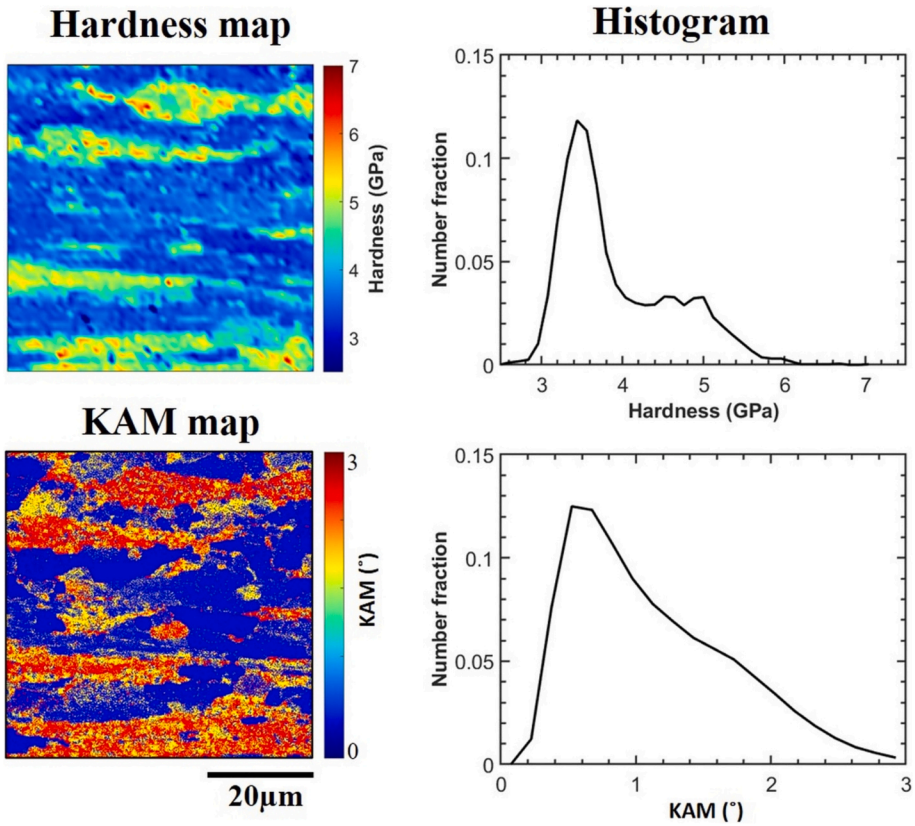

Fig. 10. Comparison of KAM and nanoindentation hardness in FP after isothermal annealing at 725 °C for 300 s.

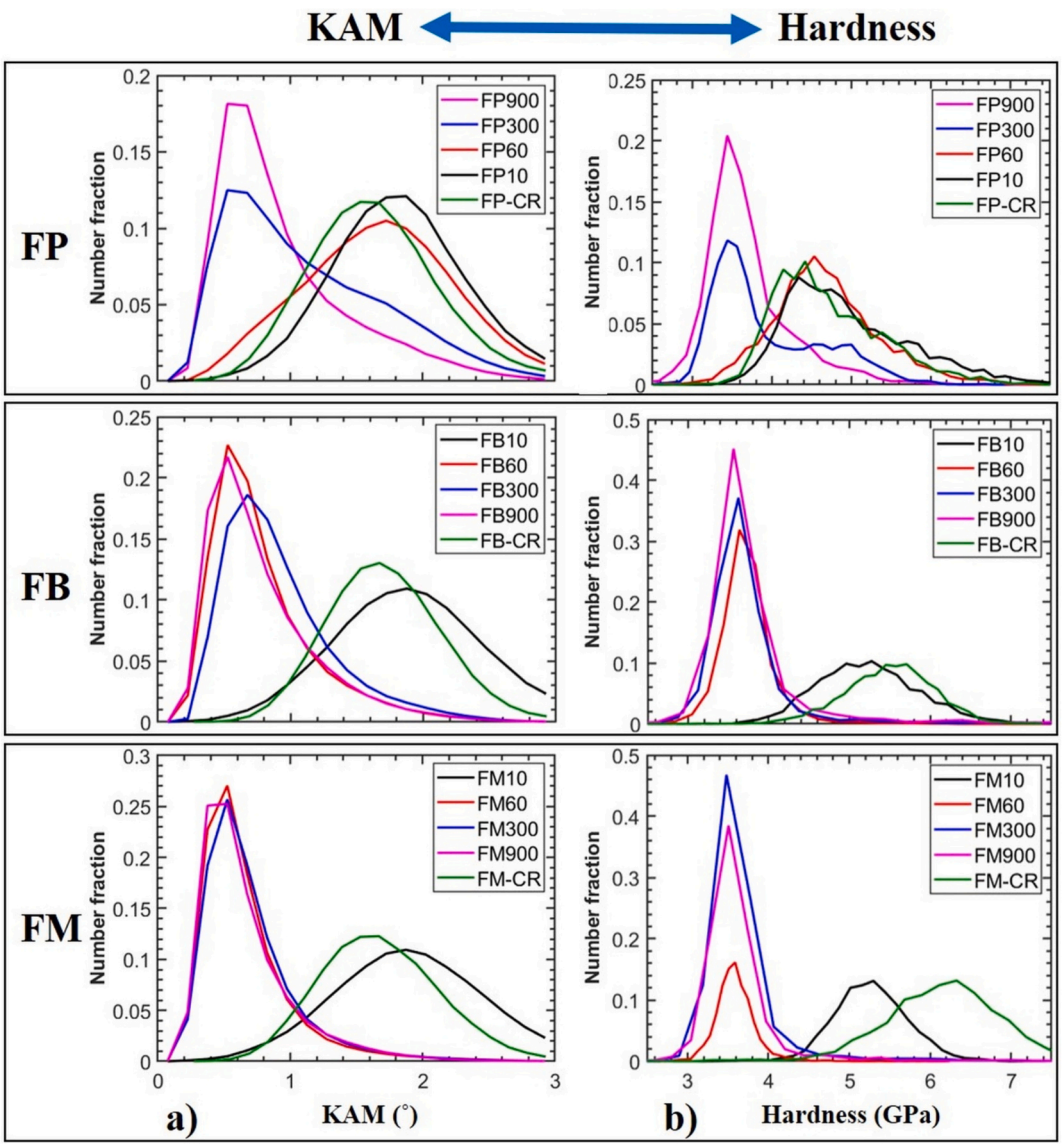

Fig. 11. Histograms of (a) KAM and (b) hardness for FP, FB and FM in the cold rolled state as well as after isothermal annealing at 725 °C for different durations.

mechanical response and the plot shows how these structural characteristics translate into material properties at the micrometer length scale.

As mentioned earlier, an analysis of all the histograms indicates that kinetics of ferrite recrystallization is similar in FB & FM and considerably faster compared to FP. Here we dwell into the underlying reasons based on the KAM and hardness measurements. One important aspect to consider in this regard is the influence of the second phase on ferrite during deformation. It is well known that non-uniform distribution of strain occurs between soft and hard phases during deformation of dual phase steels. It may be noted that FP shows a strongly banded morphology (Fig. 1), whereas FB (Fig. 2) and FM (Fig. 3) show much less banding and a more uniform distribution of the second phase. As a consequence, the length scale of the secondary constituent is smaller in the case of FB and FM. At the onset of plastic deformation, the softer phase ferrite undergoes yielding, while harder constituents / phases such as bainite and martensite continue to deform elastically. This causes heterogeneity in strain due to the higher strength of hard phases causing strain localization at the interfaces and ferrite undergoing more plastic deformation, especially in the case of FB and FM. This is confirmed by the higher overall hardness of ferrite in the case of FB and FM in the cold rolled state as shown in Fig. 11(b). Hence, higher amounts of stored energy is present in ferrite of FB and FM, which would clearly drive faster recrystallization in those cases as observed in this work.

4.2. *One-to-one structure-property correlation and properties of constituents*

In the previous section, the overall correspondence between the KAM and nanoindentation hardness was established all through the annealing process to reconcile the observed recrystallization kinetics. Here we further assess the correspondence by one-to-one correlation between KAM and hardness at the phase/constituent level. To this end, the hardness data is deconvoluted into two bins using the unsupervised K-means clustering algorithm. The KAM data is deconvoluted by considering misorientations $<1^{o}$ to be fully recrystallized. This enables a simple way to identify recrystallized portion of the map. Two examples (FP300 and FP900) are chosen to compare the deconvoluted hardness with KAM as shown in Fig. 12. The deconvoluted hardness map is shown in Fig. 12(a) and the deconvoluted KAM map is shown in Fig. 12(b). These maps show the recrystallized ferrite in blue with lower hardness and misorientation ($<1^{o}$) and unrecrystallized ferrite and secondary constituents with higher hardness and misorientation in red. Despite the inherent difference in resolution between KAM and hardness

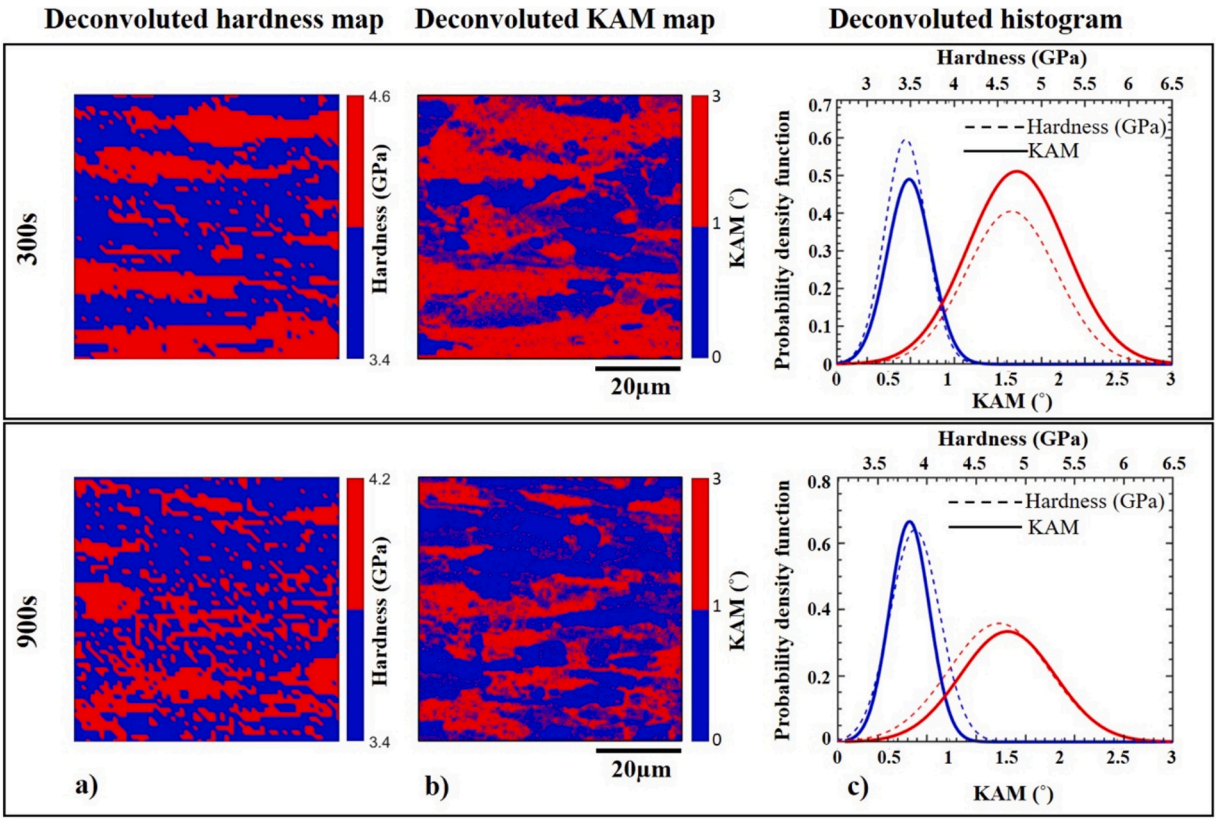

Fig. 12. Deconvoluted (a) hardness map (b) KAM map and (c) hardness and KAM histograms of recrystallized ferrite and unrecrystallized ferrite of FP after isothermal annealing at 725 °C for 300 s and 900 s. Blue colour represents recrystallized ferrite and the red colour represents unrecrystallized/partially recrystallized ferrite and pearlite. (For interpretation of the references to colour in this figure legend, the reader is referred to the web version of this article.)

measurements, good agreement can be observed between the deconvoluted maps. The corresponding histograms after deconvolution assuming a Gaussian distribution is shown in Fig. 12(c). The deconvoluted histograms of hardness and KAM are shown in a single plot for direct comparison. The dashed line represents the hardness, whereas the solid line represents the KAM. The blue coloured lines (solid and dashed) represent recrystallized ferrite, whereas the red-coloured lines (solid and dashed) represent unrecrystallized/partially recrystallized ferrite and pearlite. The plot clearly shows the excellent correlation between the hardness and KAM peaks of both the regions (recrystallized and unrecrystallized) and for both the materials (FP300 and FP900). This finding provides direct quantitative evidence for the one-to-one correlation between KAM and nanoindentation hardness in these material systems.

As a natural extension to the data presented in Fig. 12, it is instructive to compare the evolution of the hardness of ferrite during annealing in the three materials. To this end, grains of ferrite in each map are identified using the IQ based partition of the micrographs. The average hardness and KAM in each of those grains along with the scatter are then calculated and plotted against each other as shown in Fig. 13. The plot shows data from all the samples at different soaking times. Different symbols as shown in the figure are used to represent the state of the sample (cold rolled, annealing duration, etc), while different colours are used to denote the sample (FP, FB and FM). A general increasing trend in hardness with KAM is observed, as expected. Cold rolled ferrite represented by solid circles show the highest hardness and KAM, with the ferrite in FM (blue circle) showing the highest value. Interestingly, with isothermal annealing at 725 °C for 10s, the KAM values reduce (left shift) without much change in hardness indicating the onset of microstructural reengagement without change in hardness. Further annealing causes the hardness to drop and also the KAM to further reduce in the

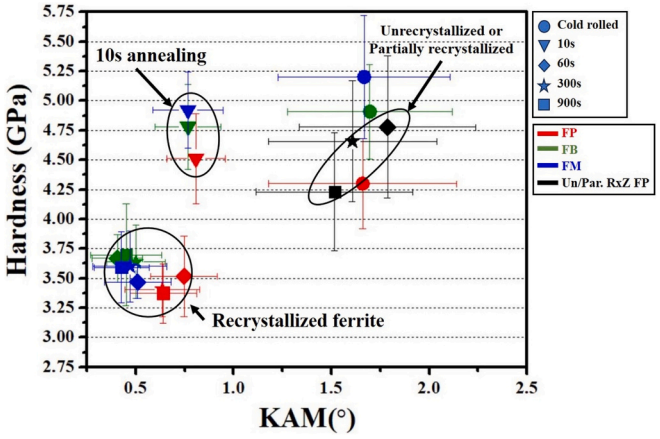

Fig. 13. Correlation between KAM and hardness of ferrite in FP, FB and FM during isothermal annealing at 725 °C.

case of FB and FM. However, in the case of FP, the ferrite hardness and KAM show a bimodal distribution with a clear distinction between recrystallized (red) and unrecrystallized or partially recrystallized grains (black symbols). This analysis not only confirms the differences in the recrystallization kinetics between the three samples presented earlier with Vickers hardness but also provides further insights as to the reasons for the differences. In summary, the one-to-one correlation between hardness and KAM obtained by coupling EBSD-KAM and nanoindentation mapping can be gainfully utilized to understand the evolution of mechanical properties at the micrometer length scale in dual phase steels.

5. Summary and conclusions

In this work, an attempt is made to the understand the microstructural changes and the associated mechanical property variations at the micrometer length scale in three different dual phase microstructures – ferrite-pearlite (FP), ferrite-bainite (FB) and ferrite-martensite (FM), all with a similar nominal chemical composition of that of DP600 grade steel. The samples were initially subjected to cold rolling followed by high temperature annealing close but below Ac1 to understand the events during recrystallization by coupling electron microscopy and nanoindentation. The following major conclusions are drawn from this work.

- ➢ Recrystallization occurs more rapidly in FM, followed closely by FB and is much slower in FP. This can be attributed to the higher density of defects present in the FM microstructure. Additionally, the uniformly distributed hard phase in FM and FB unlike the banded structure in FP serves as a significant driving force, increasing the stored energy that accelerates the recrystallization of ferrite. FB and FM samples maintained their cold rolled hardness only for 10 s of annealing before a rapid decrease in hardness. Prolonged soaking in these cases led to the formation of carbides at the boundaries of the ferrite grains. In contrast, FP sample showed a gradual decrease in hardness marked by ferrite recrystallization and cementite spheroidization.
- ➢ Very good correspondence between the EBSD-KAM maps and nanoindentation hardness maps was observed, despite the inherent differences in their native resolution.
- ➢ One-to-one correlation at the micrometer length scale between deconvoluted hardness and KAM was established from the histograms.
- ➢ The differences in the evolution of hardness and KAM of ferrite regions at the micrometer length scale during annealing was presented to demonstrate the effect of secondary constituents on the ferrite recrystallization kinetics of dual phase microstructures.

Overall, this work lays a foundation to link microstructure to the local mechanical response and thereby provide insights on the recrystallization behaviour of dual phase steels by correlative characterization, which can be gainfully used to characterize multiphase steels and ultimately fine tune the processing.

CRediT authorship contribution statement

Chavan Akash Naik: Conceptualization, Data curation, Formal analysis, Investigation, Writing – original draft. **B.K. Sarath Kumar:** Conceptualization, Data curation, Formal analysis, Investigation, Writing – original draft. **Harita Seekala:** Data curation, Investigation. **S. Janakiram:** Data curation, Investigation. **Leo A.I. Kestens:** Conceptualization, Formal analysis. **Jai Prakash Gautam:** Conceptualization, Formal analysis, Supervision, Writing – review & editing. **P. Sudharshan Phani:** Conceptualization, Data curation, Formal analysis, Methodology, Supervision, Writing – review & editing.

Declaration of competing interest

The authors declare that they have no known competing financial interests or personal relationships that could have appeared to influence the work reported in this paper.

Acknowledgements

The authors would like to thank DST FIST and DST PURSE for funding the instrumentation facility (FESEM-EBSD). SJ, PSP and JG's contribution to this work was supported by University of Hyderabad IoE research project no UoH/ IoE/RC3/21/040. CAN's contribution to this work was supported by IoE-IPDRF, University of Hyderabad.

Data availability

The data that support the findings of this study are available from the corresponding author upon reasonable request.

References

[1] N. Fonstein, Dual-phase steels*, in: Automot. Steels, Elsevier, 2017, pp. 169–216, https://doi.org/10.1016/B978-0-08-100638-2.00007-9.
[2] J.N. Hall, J.R. Fekete, 2. Steels for auto bodies: A general overview, Elsevier Ltd, 2017, https://doi.org/10.1016/B978-0-08-100638-2.00002-X.
[3] J. Drillet, V. Hébert, P. Maugis, Rolled advanced high-strength steels: in situ synchrotron X-ray di ff raction and modeling, Mater. Charact. 154 (2019) 20–30, https://doi.org/10.1016/j.matchar.2019.05.020.
[4] B. Sunil, S. Rajanna, Evaluation of mechanical properties of ferrite - martensite DP steels produced through intermediate quenching technique, SN Appl. Sci. 2 (2020) 1–8, https://doi.org/10.1007/s42452-020-03246-4.
[5] T. Ogawa, Ferrite recrystallization and austenite formation at the early stage of annealing in cold-rolled low-carbon steels, Int. J. Mech. Mater. Eng. 10 (2015), https://doi.org/10.1186/s40712-015-0049-4.
[6] Y.G. Deng, Y. Li, H. Di, Y.G. Deng, S. Key, W. Road, Y. Li, H. Di, E. Paso, E. Paso, Effect of Heating Rate during Continuous Annealing on Microstructure and Mechanical Properties of High-Strength Dual-Phase Steel, 2019, pp. 3–11, https://doi.org/10.1007/s11665-019-04253-2.
[7] H. Azizi-alizamini, M. Militzer, W.J. Poole, Formation of Ultrafine Grained Dual Phase Steels through Rapid Heating 51, 2011, pp. 958–964, https://doi.org/10.2355/isijinternational.51.958.
[8] M. Kulakov, W.J. Poole, M. Militzer, The Effect of the Initial Microstructure on Recrystallization and Austenite Formation in a DP600 Steel, 2013, https://doi.org/10.1007/s11661-013-1721-z.
[9] B. Bandi, J. Van Krevel, P. Srirangam, Interaction between ferrite recrystallization and austenite formation in dual-phase steel manufacture, Metall. Mater. Trans. A Phys. Metall. Mater. Sci. 53 (2022) 1379–1393, https://doi.org/10.1007/s11661-022-06597-2.
[10] D.Z. Yang, E.L. Brown, D.K. Matlock, G. Krauss, Ferrite Recrystallization and Austenite Formation in Cold-Rolled Intercritically Annealed Steel 16, 1985, https://doi.org/10.1007/BF02658671.
[11] K. Mukunthan, E.B. Hawbolt, Modeling recovery and recrystallization kinetics in cold-rolled Ti-Nb stabilized interstitial-free steel, Metall. Mater. Trans. A (1996), https://doi.org/10.1007/bf02595434.
[12] A.K. Rana, S.K. Paul, P.P. Dey, Effect of Martensite Volume. raction on Strain Partitioning Behavior of Dual Phase Steel 21, 2018, pp. 333–340, https://doi.org/10.1134/S1029959917040070.
[13] J. Kang, Y. Ososkov, J.D. Embury, D.S. Wilkinson, Digital image correlation studies for microscopic strain distribution and damage in dual phase steels 56, 2007, pp. 999–1002, https://doi.org/10.1016/j.scriptamat.2007.01.031.
[14] A. Varshney, S. Sangal, K. Mondal, Strain partitioning and load transfer in constituent phases in dual-phase steels, J. Mater. Eng. Perform. (2016), https://doi.org/10.1007/s11665-016-2196-z.
[15] P. Li, J. Li, Q. Meng, W. Hu, D. Xu, Effect of heating rate on ferrite recrystallization and austenite formation of cold-roll dual phase steel, J. Alloys Compd. 578 (2013) 320–327, https://doi.org/10.1016/j.jallcom.2013.05.226.
[16] S. Janakiram, P.S. Phani, G. Ummethala, H.V. Jagdeesh, S.K. Malladi, J. Gautam, L. A.I. Kestens, Insights on early recovery kinetics in ferrite - pearlite cold rolled high strength sheet steels, Mater. Charact. 193 (2022), https://doi.org/10.1016/j.matchar.2022.112332.
[17] S. Janakiram, P.S. Phani, G. Ummethala, S.K. Malladi, J. Gautam, L.A.I. Kestens, New insights on recovery and early recrystallization of ferrite-pearlite banded cold rolled high strength steels by high speed nanoindentation mapping, Scr. Mater. 194 (2021) 113676, https://doi.org/10.1016/j.scriptamat.2020.113676.
[18] C.A. Naik, B.K.S. Kumar, S. Harita, S. Roshan, S. Janakiram, P.S. Phani, J. P. Gautam, Assessment of structure-property relationships at the micrometer length scale in dual phase steels by electron microscopy and nanoindentation, Mater. Today Commun. 38 (2024) 107696, https://doi.org/10.1016/j.mtcomm.2023.107696.
[19] S. Basu, B.N. Jaya, H. Seekala, P.S. Phani, A. Patra, S. Ganguly, M. Dutta, I. Samajdar, Correlative characterization and plasticity modeling of microscopic strain localizations in a dual phase steel, Mater. Charact. 197 (2023) 112704, https://doi.org/10.1016/j.matchar.2023.112704.
[20] J. Gautam, A. Miroux, J. Moerman, L. Kestens, TNR dependent hot rolling microstructure and texture development in c-Mn dual phase and HSLA steels, Defect Diffus. Forum 391 (2019) 120–127, https://doi.org/10.4028/www.scientific.net/DDF.391.120.
[21] P. Sudharshan Phani, W.C. Oliver, A critical assessment of the effect of indentation spacing on the measurement of hardness and modulus using instrumented indentation testing, Mater. Des. 164 (2019) 107563, https://doi.org/10.1016/j.matdes.2018.107563.
[22] B. Vignesh, W.C. Oliver, G.S. Kumar, P.S. Phani, Critical assessment of high speed nanoindentation mapping technique and data deconvolution on thermal barrier

coatings, Mater. Des. 181 (2019) 108084, https://doi.org/10.1016/j.matdes.2019.108084.
[23] C.W. Price, Comments on kinetic models for recrystallization c, Scr. Mater. 19 (1985) 669–673, https://doi.org/10.1016/0036-9748(85)90359-X.
[24] B. Bandi, J. van Krevel, N. Aslam, P. Srirangam, A model and experimental validation to predict heating rates for overlap between ferrite recrystallization and austenite transformation in dual phase steel manufacture, Jom 71 (2019) 1386–1395, https://doi.org/10.1007/s11837-019-03358-2.